3D-2D Registration of Cerebral Angiograms: A Method and Evaluation on Clinical Images

Uroš Mitrović*, Žiga Špiclin, Boštjan Likar, and Franjo Pernuš

Abstract—Endovascular image-guided interventions (EIGI) involve navigation of a catheter through the vasculature followed by application of treatment at the site of anomaly using live 2D projection images for guidance. 3D images acquired prior to EIGI are used to quantify the vascular anomaly and plan the intervention. If fused with the information of live 2D images they can also facilitate navigation and treatment. For this purpose 3D-2D image registration is required. Although several 3D-2D registration methods for EIGI achieve registration accuracy below 1 mm, their clinical application is still limited by insufficient robustness or reliability. In this paper, we propose a 3D-2D registration method based on matching a 3D vasculature model to intensity gradients of live 2D images. To objectively validate 3D-2D registration methods, we acquired a clinical image database of 10 patients undergoing cerebral EIGI and established "gold standard" registrations by aligning fiducial markers in 3D and 2D images. The proposed method had mean registration accuracy below 0.65 mm, which was comparable to tested state-of-the-art methods, and execution time below 1 s. With the highest rate of successful registrations and the highest capture range the proposed method was the most robust and thus a good candidate for application in EIGI.

Index Terms—Cerebral angiograms, evaluation, gold standard, image-guided interventions, 3D-2D registration.

I. INTRODUCTION

IN RECENT years, minimally invasive endovascular image-guided interventions (EIGIs) have been developed for treatment of many types of cerebrovascular diseases like stenosed or totally occluded vessels, aneurysms, tumor beds, or arteriovenous malformations (AVMs). To reliably quantify the site, form and extent of a vascular anomaly and to plan the intervention, 3D images are acquired prior to EIGI either by computed tomography angiography (CTA), magnetic resonance angiography (MRA), or more recently by 3D rotational angiography (3DRA) and digitally subtracted 3DRA (3D-DSA) using a C-arm. An EIGI is guided by low dose 2D X-ray fluoroscopic images which have excellent spatial and temporal resolution,

but unfortunately lack contrast and especially depth information. During EIGI the vasculature is occasionally emphasized by injecting a contrast agent into the bloodstream; however, its excessive use may result in hazardous patient reactions.

Navigation and optimal application of devices in 3D based on observing 2D images demand considerable skills in mental reconstruction of a 3D scene and image-hand coordination. An emerging technical solution is to exploit the positive aspects of 3D and 2D images by fusing the static 3D information with the temporal information of the live 2D fluoroscopic images [1], [2]. The fused 3D and 2D data may be exploited in two ways. First, by projecting static 3D data like (segmented) vessels, associated pathology and important surrounding tissue and/or treatment plan onto the live 2D fluoroscopic images obtained under any C-arm projection angle. Second, by back-projecting the dynamic information in live 2D fluoroscopic images, like the position of devices and the propagation of contrast agent, onto the 3D image. The immediate clinical benefits of both strategies are more accurate navigation and reduction of X-ray dose and harmful contrast agent. Additionally, the second strategy may further improve diagnosis and lead to better intervention planning and intra- and post- intervention evaluation. A good spatial alignment of 3D and 2D images, however, is crucial to all strategies of fusion and can be achieved by 3D-2D image registration.

Before a 3D-2D image registration method can be incorporated into an EIGI workflow, it must undergo extensive validation because the sources of alignment errors and uncertainties are numerous. Objective and thorough validation and comparison to state-of-the-art methods requires acquisition of validation image datasets, definition of corresponding "gold standard" registration and its accuracy, and design of validation protocol and metrics. To the best of our knowledge, no clinical image datasets with "gold standard" registrations are publicly available for validating 3D-2D registrations of cerebral angiograms.

A. Related Work

Registration of live 2D fluoroscopic images with 3D CTA, MRA, or 3D-DSA images belongs to the category of 3D-2D (often also 2D-3D) registrations, and has been studied not only in the context of endovascular interventions, but even more deeply in the contexts of image-guided radiation therapy and image-guided minimally invasive therapies. Recently, we have comprehensively surveyed the 3D-2D registration methods [3]. The methods are mainly characterized by the nature of registration basis and dimensional correspondence. According to the nature of registration basis, 3D-2D image registration methods can be categorized as calibration-based and extrinsic or intrinsic image-based methods. Dimensional correspondences

are established either by the projection, back-projection, or reconstruction strategies. Here, we limit the review of 3D-2D registration methods to those that have been proposed for registering images of vasculature.

Most calibration-based methods [4], [5] are limited to 3D-DSA to fluoroscopy registrations as they are based on the geometry of a calibrated C-arm X-ray angiography device. Because the 3D-DSA image is obtained with the same device as the 2D fluoroscopic images, registration can be calculated on the basis of the imaging geometry and calibration data. However, even small patient movements between the acquisition of the 3D-DSA and fluoroscopic images may hamper the calibration-based registration, which limits its use in EIGI.

Extrinsic image-based methods [6] rely on artificial objects like stereotactic frames or a small number of markers attached to frames, catheters, or implanted into bone, soft tissue, or skin-affixed. While stereotactic frames and bone implanted markers are rigidly attached, skin markers and markers implanted into soft tissue can move due to skin elasticity or soft tissue deformation. Besides, registrations are generally accurate only over the region covered by the markers.

Intrinsic image-based registration methods rely solely on vasculature information in 3D and 2D images. The 3D-DSA, CTA, and MRA are standard acquisition techniques that clearly reveal the vasculature, while in the live 2D fluoroscopic images the vasculature is made visible by contrast agent injection. This is probably not a drawback of intrinsic methods, as contrast agent is routinely injected several times during EIGI, e.g., for navigation and blood flow visualization. The intrinsic image-based methods are further categorized as intensity-, feature-, and gradient-based or hybrid methods [3].

Intensity-based 3D-2D registration methods [7]–[13] are typically based on 2D-2D matching of real fluoroscopic and simulated images, called digitally reconstructed radiographs (DRRs), obtained by casting virtual rays through a CTA, MRA, or 3DRA image. The most frequently used similarity measures for these methods are mutual information, cross correlation, pattern intensity, gradient correlation and gradient difference. Hipwell *et al.* [9] analyzed six different similarity measures and showed that pattern intensity and gradient difference gave the best results. Van der Bom [12] analyzed seven different optimizers and three different similarity measures and showed that the combination of Powell's optimization method and gradient correlation was optimal. McLaughlin *et al.* [11] compared an intensity-based method using gradient difference and a feature-based registration method [14] and showed that the former was more accurate and reliable but significantly slower. Owing to DRR generation, high computational complexity is characteristic of intensity-based methods.

Feature-based methods [14]–[20] rely on matching corresponding features extracted from 3D and 2D images. Feldmar *et al.* [16] modeled vessels as curves in 3D and 2D and matched the curve points and orientations using the iterative closest point (ICP) framework. To speed-up ICP matching, Rivest-Hénault *et al.* [20] precomputed a modified distance transform of a segmented vessel tree. Groher *et al.* [17] used branching points and topology of the segmented vessel tree as features in a modified ICP framework. In [18] the method in [17] was extended to a maximum likelihood segmentation-registration framework that projects the 3D skeleton of the vessel tree to 2D so as to initialize and execute the 2D segmentation. The 2D skeleton obtained from the segmented image is registered with the projection of the 3D skeleton. The advantage of feature-based methods is their low computational complexity because of large data reduction. Unfortunately, the accuracy of these methods depends directly on the quality of segmentation by which features are extracted. Besides, segmentation of live 2D images may be too time consuming to allow clinical use of feature-based methods.

Gradient-based methods [21] are based on the fact that rays emanating from the X-ray source and pointing to edges in the X-ray image are tangent to surfaces of distinct anatomical structures [22]. Recently, Mitrovic *et al.* [21] applied a gradient-based 3D-2D registration method [23] to cerebral vessels. Computational demands are usually lower than in intensity-based methods since only a certain number of significant volume gradients is processed. However, the gradient matching process is driven mainly by gradient magnitude information, which is sensitive to spatial variations of image contrast. Besides, one-to-one gradient matching is sensitive to small image transformations and thus not very robust.

The registration methods that use a mixed registration basis are referred as hybrid methods [2], [24]–[30]. Turgeon *et al.* [26] registered a triangulated mesh model of vasculature, extracted from a pre-EIGI 3D image by multiscale segmentation, to segmented 2D image(s) by using entropy correlation coefficient as similarity measure. Similarly, Copeland *et al.* [2] created a triangular mesh of vasculature using Marching cubes segmentation that was projected and correlated to enhanced 2D time series. Ruijters *et al.* [25] registered the 2D distance transform of a projected skeleton of the pre-EIGI 3D image to the vessel enhanced 2D fluoroscopic image using the dot-product of the two images as similarity measure. Jomier *et al.* [27] projected each 3D vessel centerline point onto the 2D-DSA image and smoothed the intensities in the projected point's neighborhood proportionally to the corresponding vessel radius. The similarity measure for 3D-2D registration was the sum of smoothed intensities at the projected centerline points, weighted by corresponding vessels's radii. Typically, the hybrid methods mimic the intensity-based methods, but approximate or even avoid DRR generation and, instead, employ efficient methods for projecting 3D information to 2D.

For validating the 3D-2D image registration methods there exist four publicly available image datasets, two of cadaveric spine segments [31], [32] one of a porcine cadaver head [33] and one with synthetic spine and pelvis images generated from the Visible Human data [34]. Quite accurate reference (or "gold standard") registrations are available for all four datasets, as they were obtained using fiducial markers [31], [33], knowledge of image acquisition geometry and intensity based registration [32] and knowledge of image generation geometry [34]. The problem with these datasets is that clinical realism is captured only to a limited extent, except for the porcine cadaver head image dataset, and that images do not capture the rich biological variability, which can be captured only by imaging a large number of patients. Besides, validation of a 3D-2D regis-

tration method has to be performed according to a clinical context. The clinical context associated with the publicly available image datasets is spine surgery [31], [32], [34], and radiotherapy of the head [33]. For other clinical contexts such as (cerebral) EIGI, to the best of our knowledge, no validation datasets exist.

B. Motivation and Our Approach

The main motivation for this work is twofold. First, in most of the reviewed references the authors primarily aim to achieve a high level of accuracy of their 3D-2D registration method. The reviewed methods typically achieved mean registration accuracy below 1 mm that is probably acceptable for EIGI. However, their rather low computational efficiency and, especially, robustness limit their application in EIGI. Robustness of a method may also depend on the anatomy to which it is applied, e.g., methods [8], [17]–[19], [27], [28] that were developed to register images of larger vasculatures in the abdominal area may not be equally robust on images of cerebral vasculature. Our first goal was, therefore, to develop a computationally efficient and, more importantly, a robust 3D-2D registration method. Second, to objectively quantify the performance of 3D-2D registration methods, with special attention dedicated to quantification of robustness, realistic validation image datasets in the context of EIGI have to be available. Our second goal was thus to acquire a large enough clinical image database.

In this paper, based on our previous work in [29], we develop a hybrid 3D-2D registration method, in which features extracted from the pre-EIGI 3D image are matched directly to information contained in live 2D images. Matching is based on comparison of orientations at vessels' centerline points, projected from 3D to 2D, to orientations of live 2D image(s) intensity gradients within a certain neighborhood around a projected centerline point. The idea of matching 3D vessel orientations to orientations of 2D intensity gradients was inspired by computer vision community [35], [36] where several studies demonstrated robust matching of corresponding orientation features. Such a 3D-2D registration is expected to be robust to significant variations of image contrast that are characteristic of cerebral angiograms.

To extensively and objectively validate the novel method and compare it to state-of-the-art methods, we have acquired a clinical image database comprised of 10 image datasets of patients undergoing cerebral-endovascular treatment. Eight patients underwent aneurysm treatment and two underwent AVM embolization. The degree of the cerebrovascular pathologies varied considerably between the patients. Accurate "gold standard" 3D-2D registrations relating any point in the pre-EIGI 3D image to its corresponding point on a 2D view requires a retrospective calibration of the C-arm imaging system and a retrospective positioning of the pre-EIGI 3D image in the patient space. These two tasks were simultaneously achieved by aligning fiducial markers attached to patients and visible both in 3D and 2D images. We believe that 10 clinical image datasets acquired in the context of cerebral EIGI enable an objective and thorough evaluation of novel and state-of-the-art 3D-2D registration methods.

C. Contributions

The work presented in this paper makes several methodological, data, and validation contributions.

1) A novel, accurate, robust, and fast method for 3D-2D rigid registration of cerebral angiograms is presented in Section II,
2) A database of real clinical images prepared purposely for quantitative evaluation of the performances of 3D-2D rigid registration methods is presented in Section III,
3) Extensive and objective validation of the novel method and its comparison to state-of-the-art intensity-, feature-, and gradient-based 3D-2D registration methods is presented in Sections IV and V.

II. METHOD

C-arm imaging is modeled as a perspective projection, the parameters of which can be estimated through a calibration procedure. Calibration is required prior to 3D-2D registration so that the exact position and orientation of the C-arm imaging system in some world (patient) coordinate system (S_w) is known (Fig. 1). The result of C-arm calibration is a 3×4 projection matrix $\mathbf{P}$, which relates any 3D point in $\mathbf{S}_w$ to its corresponding 2D point on detector plane defined by the coordinate system S_s. To position the coordinate system of a pre-EIGI 3D image $(\mathbf{S}_v)$ in $\mathbf{S}_w$ so that corresponding cerebrovascular structures on the projected 3D and live 2D image(s) overlap, one has to find an optimal transformation $\mathbf{T}(\mathbf{q})$ $(4 \times 4$ matrix) defined by six rigid-body parameters $\mathbf{q} = (t_x, t_y, t_z, \omega_x, \omega_y, \omega_z)$.[1] Hence, a registration method is required that relates the pre-EIGI 3D image and the live 2D image(s) acquired by the C-arm imaging system.

The 3D-2D registration method we propose employs feature extraction from the pre-EIGI 3D image followed by matching of these features to the information in live 2D image(s). In feature extraction, the information on vasculature in the pre-EIGI 3D image is compressed to a 3D vessel tree model, which is described by geometric primitives (GPs) that can be efficiently projected from 3D to 2D. Geometric primitives describing the 3D vessel tree are the vessels' centerline points, orientations and radii. The alignment of 3D and 2D image(s) is achieved by matching projected GPs to intensity gradients of live 2D image(s). In the following, the 3D vessel tree model and the GP matching process are described.

A. 3D Vessel Tree Model

A 3D vessel tree is modeled with a set of GPs: $\{\mathrm{GP}_i\} = \{\mathbf{C}_i^{3D}, \mathbf{V}_i^{3D}, R_i\}$, $i = 1, 2, \ldots, N$, where $\mathbf{C}_i^{3D}$ are points on the vessels' centerlines and $\mathbf{V}_i^{3D}$ and R_i are the associated orientations and radii, respectively (Fig. 1). The GPs are obtained in four steps.

1) Segmentation of the pre-EIGI 3D image by a manually determined global threshold and selection of the largest connected component as the output of segmentation.
2) Skeletonization using Lee's thinning algorithm [37] to obtain the vessels' centerline points $\mathbf{C}_i^{3D}$.

---

[1] It is assumed that the cerebral vasculature is a rigid structure.
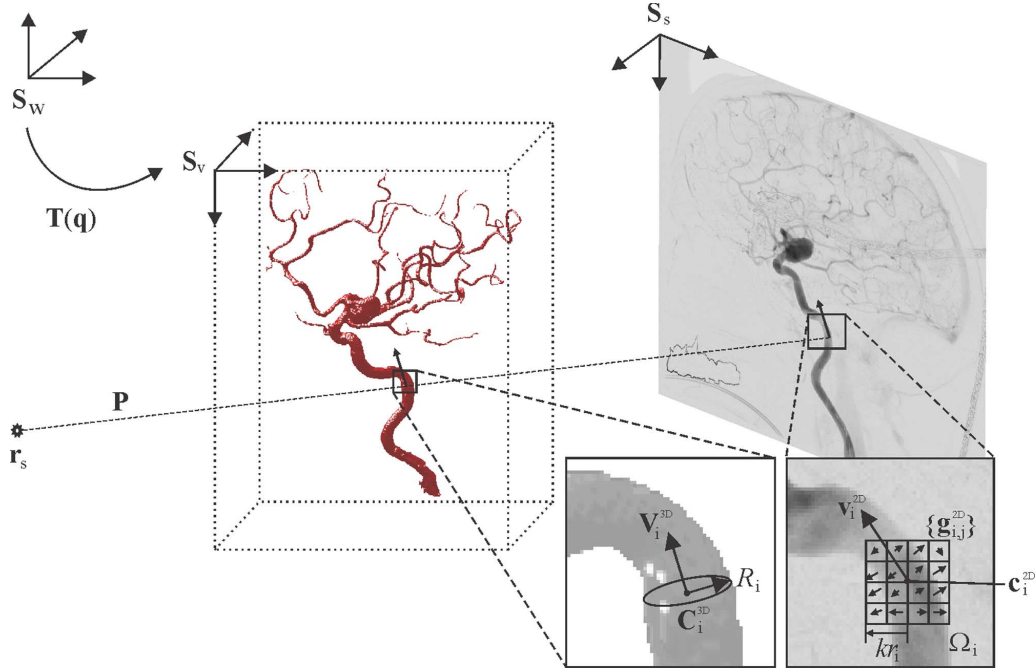
Fig. 1. Geometrical setup of 3D-2D registration and the basic principle of the proposed 3D-2D image registration method.

3) Hessian analysis in the scale-space of 3D neighborhood of each centerline point $\mathbf{C}_i^{3D}$ to obtain, at the scale of maximum medialness response, the vessels' orientations $\mathbf{V}_i^{3D}$ as the eigenvector of the Hessian matrix associated with the largest eigenvalue and the vessels' radii R_i[38].

4) Elimination of incorrect GPs related to false branches in the 3D skeleton [17] and elimination of unreliable GPs such as branching points without a unique orientation $\mathbf{V}_i^{3D}$.

The vessels' centerline points, the corresponding orientations and radii could also be obtained in other ways [39], [40].

B. Matching of Geometrical Primitives

The 3D-2D registration method is based on matching orientations $\mathbf{V}_i^{3D}$ of the 3D vessel tree model, which point in the direction of the vessel at points $\mathbf{C}_i^{3D}$ and orientations of corresponding 2D intensity gradients of live 2D image(s), which point in directions of largest intensity increases.

Let $\Omega = \{\mathbf{x}\}$ denote the 2D image domain on which the intensity gradients $\mathbf{g}^{2D}$ are defined. Dimensional correspondence between the GPs that are defined in 3D and the intensity gradients $\mathbf{g}^{2D}$ that are defined in 2D is obtained by 3D to 2D projection of GPs

$$\mathbf{c}_i^{2D} = \mathrm{P} \cdot \mathrm{T}(\mathbf{q}) \cdot \mathbf{C}_i^{3D} \tag{1}$$
$$\mathrm{v}_i^{2D} = \mathrm{P} \cdot \mathrm{T}(\mathbf{q}) \cdot (\mathbf{C}_i^{3D} + \mathbf{V}_i^{3D}) - \mathbf{c}_i^{2D}. \tag{2}$$

By assuming that the orthogonal vessel cross sections are round, each radius R_i in 3D scales to a radius r_i in 2D as

$$r_i = \frac{|\mathbf{r}_s - \mathbf{c}_i^{2D}|}{|\mathbf{r}_s - \mathbf{C}_i^{3D}|} R_i \tag{3}$$

where r_s is the position of the X-ray source, $|\mathbf{r}_s - \mathbf{C}_i^{3D}|$ and $|\mathbf{r}_s - \mathbf{c}_i^{2D}|$ are source-to-centerline point and source-to-projected centerline point distances, respectively, and $|\cdot|$ is the L_2 norm.

To reduce the influence of high magnitude gradients on the matching process and to reduce the sensitivity to changes of image contrast and to small image transformations, we employ a neighborhood-based matching of orientations $\mathbf{v}_i^{2D}$ to the orientations of $\mathbf{g}^{2D}$. For each $\mathbf{v}_i^{2D}$ a set of intensity gradients $\{\mathbf{g}_{i,j}^{2D}\}$, $j = 1, 2, \ldots, M_i$, is computed in a square neighborhood Ω_i of $\mathbf{c}_i^{2D}$, where $\Omega_i = \{\mathbf{x}_{i,j}; |\mathbf{c}_i^{2D} - \mathbf{x}_{i,j}|_\infty \leq k r_i\}$. Here, the parameter $k > 0$ controls the size of the neighborhood. The degree of matching between the orientations of $\mathbf{v}_i^{2D}$ and $\{\mathbf{g}_{i,j}^{2D}\}$ is measured by the following similarity measure (SM)

$$\mathrm{SM} = \frac{\sum_{i=1}^N \sum_{j=1}^{M_i} f(\alpha_{i,j})}{\sum_{i=1}^N M_i} \tag{4}$$

where $f(\alpha_{i,j})$ is the angle weighting function

$$f(\alpha_{i,j}) = \begin{cases} |\sin^n(\alpha_{i,j})|, & |\mathbf{g}_{i,j}^{2D}| \geq \beta \\ 0, & \text{otherwise} \end{cases} \tag{5}$$

and $\alpha_{i,j}$ denotes the angle between the ith unit vector $\mathbf{v}_i^{2D}$ and the jth intensity gradient $\mathbf{g}_{i,j}^{2D}$ contained in Ω_i

$$\alpha_{i,j} = \arcsin\left(\frac{|\mathbf{V}_i^{2D} \times \mathbf{g}_{i,j}^{2D}|}{|\mathbf{V}_i^{2D}||\mathbf{g}_{i,j}^{2D}|}\right). \tag{6}$$

To make the matching process more robust, the angle weighting function in (5) employs two outlier rejection criteria. The first determines a set of so-called *plausible matches*, while the second controls the sensitivity of $f(\alpha_{i,j})$ to *weak matches*. A plausible match is represented by a high magnitude gradient $\mathbf{g}_{i,j}^{2D}$ and is determined according to the threshold parameter $\beta = |\mathbf{g}_m^{2D}|$, where $|\mathbf{g}_m^{2D}|$ is the mth percentile of the magnitude distribution of $\mathbf{g}^{2D}$. A weak match, i.e., a higher deviation of $|\alpha_{i,j}|$ from $\pi/2$, is penalized by parameter n in the power of the sine function in (5).
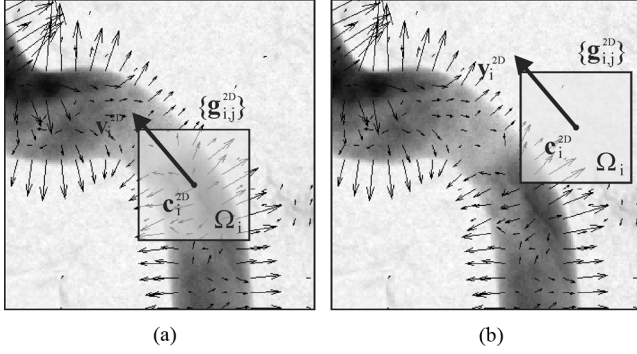
Fig. 2. Intensity gradients $\{g_{i,j}^{2D}\}$ and projected GPs $\{c_i^{2D}, V_i^{2D}\}$ in a "gold standard" (a) and displaced from "gold standard" position (b).

Fig. 2 illustrates the reasoning behind the proposed SM in (4). When the pre-EIGI 3D image is optimally aligned with the live 2D image, the c_i^{2D} and v_i^{2D} model the position and orientation of a local centerline of the underlying 2D vessel, respectively [Fig. 2(a)]. In this case v_i^{2D} is perpendicular to most of the high intensity gradients in $\{g_{i,j}^{2D}\}$. If the pre-EIGI 3D image is not optimally aligned, only a part of the vessel is within the GP's neighborhood Ω_i [Fig. 2(b)]. In this case, the plausible and strong matches between orientations v_i^{2D} and corresponding gradients in $\{g_{i,j}^{2D}\}$ will guide the registration in such a way that c_i^{2D} will move closer to the vessel's centerline. Matching is performed iteratively, by searching in each iteration for such rigid-body parameters $q*$ that maximize the SM

$$q^* = \arg\max_{q} \mathrm{SM}. \tag{7}$$

When two live 2D images are available during EIGI, then the overall SM is simply the sum of individual SMs.

C. Implementation Details

The extraction of the 3D vessel tree model (Section II-A) required by the proposed MGP method typically resulted in $N = 1700$ GPs. During 3D-2D registration GPs were matched to 2D intensity gradients g^{2D} using the SM in (4). For each GP projected from 3D to 2D, the angle weighting function (5) was evaluated between the GP and all $\{g_{i,j}^{2D}\}$ in a square neighborhood Ω_i. For a particular choice of $n = 2$ in (5), which yielded good registration performances as shown in Section V-B, the sum of $f(\alpha_{i,j})$ over the square neighborhood Ω_i was efficiently computed by using integral images [41]. First the intensity gradients $g^{2D} < \beta$ were set to zero and the remaining intensity gradients were normalized to unit length and denoted $\bar{g}^{2D}$. Note that the projected GPs v_i^{2D} were of unit length. Let $(u,v)\epsilon\Omega$ indicate pixel indices along horizontal and vertical 2D image axes, respectively, and $\bar{g}_{i,j}^{2D} = [gu_{i,j}\ gv_{i,j}]^T$ and $v_i^{2D} = [vu_i\ vv_i]^T$. If n is set to 2, the sum in the numerator of (4) expands to

$$\sum_{j=1}^{M_i} f(\alpha_{i,j}) = \sum_{j=1}^{M_i} |v_i^{2D} \times g_{i,j}^{-2D}|^2$$

$$= vv_i^2 \sum_{j=1}^{M_i} gu_{i,j}^2$$

$$- 2vu_I vv_i \sum_{j=1} gu_{I,j} gv_{I,j}$$

$$+ vu_i^2 \sum_{j=1} gv_{i,j}^2. \tag{8}$$

Three integral images for corresponding three expanded sums over j-s in (8) can be computed as [41]

$$s(u,v;g) = g(u,v) + s(u-1,v;g)$$
$$+ s(u,v-1;g) - s(u-1,v-1;g) \tag{9}$$

where $g = \{gu^2, gv^2, gu \cdot gu\}$. The integral image $s(u,v;g)$ is 0 for $u,v < 0$. For each of the N projected GPs, i.e., v_i^{2D}, the corresponding three sums for g are evaluated as

$$\sum_{j=1}^{M_i} g = s(u_i + r_i, v_i + r_i; g)$$

$$- s(u_i - r_i - 1, v_i + r_i; g)$$
$$- s(u_i + r_i, v_i - r_i - 1; g)$$
$$+ s(u_i - r_i - 1, v_i - r_i - 1; g) \tag{10}$$

where (u_i, v_i) is the location of projected 3D centerline point c_i^{2D}. It follows from (10) that for each g the sum over neighborhood Ω_i can be computed only by three add/subtract operations and is independent of the neighborhood size r_i. Hence, (8) can be computed in only 15 multiply-add-subtract operations.

III. MATERIALS

A. Clinical Image Database

The clinical image database contained 10 image datasets of patients undergoing cerebral-endovascular treatment. Images were acquired just before the start of the treatment, while patients were in deep anesthesia. The catheter was present in all of acquired images. Eight patients underwent aneurysm treatment and two underwent AVM embolization. The degree of cerebrovascular pathologies varied considerably between the patients (Fig. 3). The images were acquired on a Siemens Axiom Artis dBA biplane flat panel detector angiography system. For each patient two pre-EIGI rotational scans of the head were first acquired, one with and one without contrast agent, which resulted in two respective cone-beam computed tomography (CBCT) volumes. The CBCT volumes were subtracted to obtain a 3D digitally subtracted angiogram (3D-DSA) with high vessel contrast. The CBCTs and the resulting 3D-DSA images had voxel sizes of $0.46 \times 0.46 \times 0.46$ mm and dimensions of $512 \times 512 \times 391$. Next, two 2D fluoroscopic (2D-MAX) and two 2D-DSA images were acquired from two views, one in pure lateral (LAT) and the other approximately in anterior-posterior (AP) gantry position. Compared to 2D-DSA images, the 2D-MAX images manifested lower vessel contrast and also depicted nonvascular anatomical structures and interventional tools. The 2D images had pixel sizes of 0.154×0.154 mm and dimensions of either 1920×1920 or 2480×1920 pixels.

Prior to 3D-2D registration each 3D-DSA image was blurred with a Gaussian filter ($\sigma = 0.5$ mm) and resampled to isotropic resolution of 0.75 mm. The live 2D images were blurred with
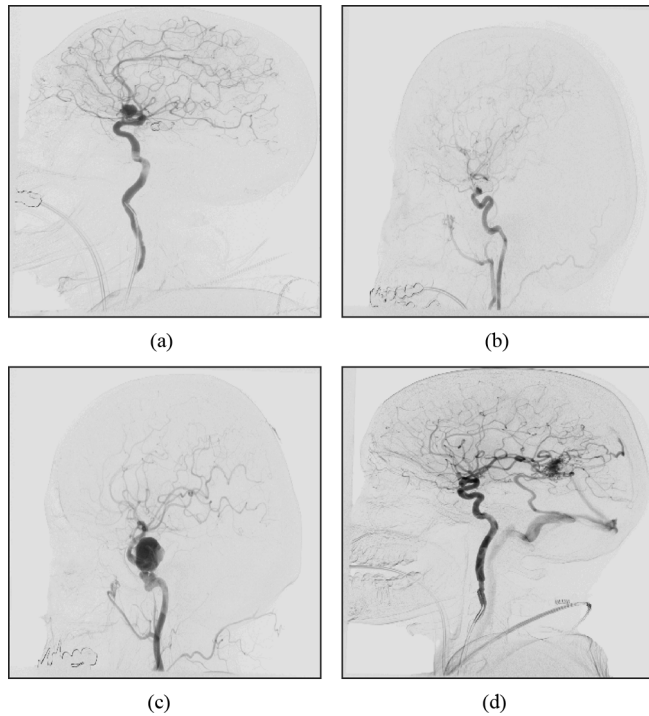
Fig. 3. Characteristic lateral 2D-DSA clinical images. Patients 3 (a), 5 (b), and 7 (c) underwent aneurysm treatment, while patient 8 (d) underwent AVM treatment.

a Gaussian filter ($\sigma = 0.5$ mm) and resampled to the isotropic resolution of 0.3 mm. In each 3D-DSA image a volume of interest (VOI) was defined as the bounding box containing the segmented 3D vessel tree, while in each 2D image a rectangular region of interest (ROI) containing the entire cerebral vasculature was defined manually. All 3D-2D registration methods were applied to resampled 3D and 2D images and corresponding VOIs and ROIs because of the high computational complexity of the intensity-based method.

B. "Gold Standard" Registration

Since the acquired clinical image datasets will be used for comparative evaluations of 3D-2D registration methods, an accurate reference transformation (or a "gold standard" transformation) of any point in the pre-EIGI 3D image to its corresponding point on a 2D view needs to be known. This requires retrospective calibration of the C-arm imaging system and a retrospective positioning of the pre-EIGI 3D image in the patient space. These two tasks were simultaneously achieved by aligning fiducial markers attached to patients and visible both in 3D and 2D images.

During the acquisition of 3D and 2D images, each patient wore an elastic headband with 12 ($N_M = 12$) integrated 2-mm-diameter steel ball bearings, which served as fiducial markers (Fig. 4). The centroid of the 12 fiducial markers approximately coincided with the centroid of the cerebral vasculature. In this way, the alignment based on fiducial markers should achieve the highest accuracy near the centroid of the cerebral vasculature [42]. The centers of fiducial markers were extracted from all CBCTs without contrast agent and 2D-MAX images by using

the intensity centroid method [43], [44]. As the presence of fiducial markers on the 3D and 2D images can bias the 3D-2D registrations, the areas of fiducial markers were removed from the 3D and 2D images after obtaining the "gold standard." Intensities in the removed areas were substituted using spline interpolation [8] [Fig. 4(d)].

Aligning the centers of fiducial markers in 3D and 2D images involves finding the projection matrix $\mathbf{P}$ of the C-arm imaging system for each 2D view and finding the optimal transformation $\mathbf{T}(\mathbf{q})$ of the 3D image. The projection matrix $\mathbf{P}$ can be defined by six geometric parameters of the C-arm imaging system, i.e., source-to-object (SOD) and source-to-detector distances (SID), primary (PA), and secondary angles (SA) of the C-arm gantry and coordinates of the principle point (u_0, v_0) on the flat panel detector

$$\mathbf{P} = \begin{bmatrix} -\text{SID} & 0 & -u_0 \\ 0 & -\text{SID} & -v_0 \\ 0 & 0 & 1 \end{bmatrix} \left[\mathbf{R}_{\text{PA}} \mathbf{R}_{\text{SA}} \middle| \begin{matrix} 0 \\ 0 \\ -\text{SOD} \end{matrix} \right] \quad (11)$$

where $\mathbf{R}_{\text{PA}}$ and $\mathbf{R}_{\text{SA}}$ are 3×3 rotation matrices defined by the PA and SA angles [45].

The projection matrices of LAT and AP 2D views, $\mathbf{P}_{\text{LAT}}$ and $\mathbf{P}_{\text{AP}}$, and the epipolar geometry [46] can be used to reconstruct in 3D the centers of fiducial markers $\mathbf{X}_{\text{ci}}^{\text{R}}$ from their corresponding 2D centers. The reconstructed centers $\mathbf{X}_{\text{ci}}^{\text{R}}$ and centers of fiducial markers $\mathbf{X}_{\text{ci}}$ extracted from a 3D image were aligned by minimizing the fiducial registration error (FRE)

$$\text{FRE} = \sqrt{\frac{1}{N_M} \sum_{i=1}^{N_M} (\mathbf{X}_{\text{ci}}^{\text{R}}(\mathbf{P}_{\text{LAT}}, \mathbf{P}_{\text{AP}}) - \mathbf{T}(\mathbf{q})\mathbf{X}_{\text{ci}}).} \quad (12)$$

The rigid transformation $\mathbf{T}(\mathbf{q})$ that minimizes FRE was computed by singular value decomposition. Approximate values of the $12(6+6)$ geometric parameters defining the projection matrices $\mathbf{P}_{\text{LAT}}$ and $\mathbf{P}_{\text{AP}}$ were obtained from the DICOM header of corresponding 2D images and were refined by minimizing FRE. In total $18(6+6+6)$ parameters were optimized, resulting in optimal LAT and AP projection matrices and optimal rigid transformation $\mathbf{T}(\mathbf{q})$ that represented the "gold standard" registration of each of the 10 clinical image datasets.

Based on the established methodology proposed by Fitzpatrick *et al.* [42] the FRE can be used to predict the mean target registration error (mTRE) for any target of interest. As the target points we have used the 3D vessels' centerline points $\mathbf{c}_i^{\text{3D}}$. The obtained FREs ranged from 0.038 to 0.060 mm, while the predicted mTREs that represent the accuracy of computed "gold standard" registration ranged from 0.033 to 0.056 mm, which indicated a highly accurate "gold standard."

IV. EXPERIMENTS

The clinical image database was used to quantitatively evaluate the performances of the proposed and three state-of-the-art 3D-2D registration methods Table I. Selection of the state-of-the-art methods was limited to methods that are well established in the field of 3D-2D registrations, and that are capable of registering a 3D image either to one 2D view or to multiple 2D views simultaneously. The first of the state-of-the-art methods
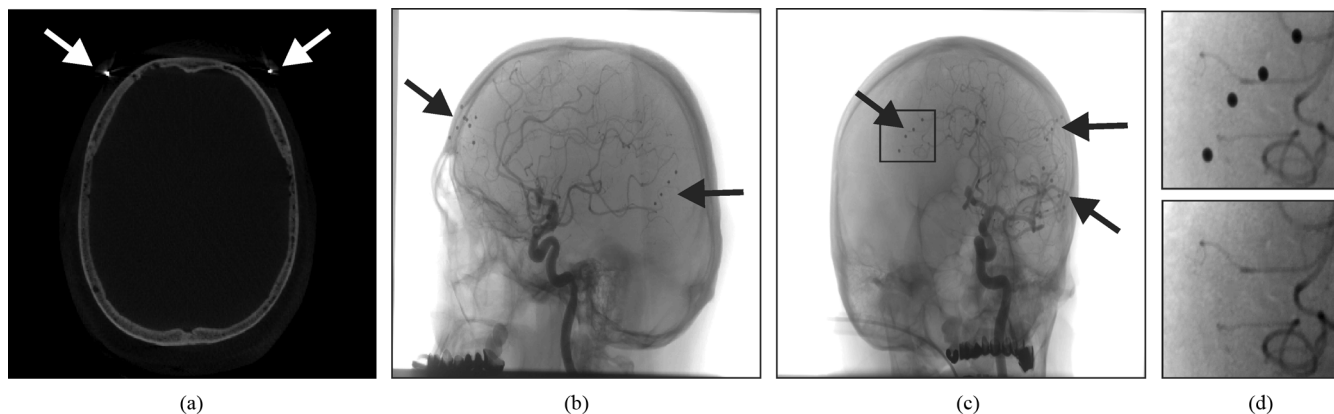
Fig. 4. Typical 3D and 2D images with fiducial markers: a CBCT axial slice (a), a 2D-MAX LAT (b) and 2D-MAX AP (c) images. The *arrows* indicate the locations of the fiducial markers. The *rectangular area* in (c) is shown enlarged in (d) *top*, while (d) *bottom* is obtained after substituting the intensity information in the areas of fiducial markers by spline interpolation.

TABLE I
EVALUATED 3D-2D REGISTRATION METHODS CLASSIFIED BY THE
REGISTRATION BASIS, DIMENSIONAL CORRESPONDENCE AND APPLICATION

Method	Registration basis	Dimensional correspondence	Application
MIP-MI [9], [47]	Intensity-based	Projection	General
ICP [20]	Feature-based	Projection	Vascular
BGB [22]	Gradient-based	Back-projection	General
MGP (Proposed method)	Hybrid	Projection	Vascular

was the intensity-based method that used maximum intensity projection (MIP) images. MIPs were used instead of DRRs to suppress subtraction artifacts and intensity inhomogeneities and to obtain a simulated 2D-DSA image with high vessel-to-background contrast. Among the state-of-the-art similarity measures [9] mutual information (MI) performed best on our clinical database, thus results are presented only for the MI-based method, referred to as MIP-MI. The second was the iterative closest point (ICP) matching between the projected 3D and the 2D vessel tree centerline points [20]. The third method was the back-projection gradient-based (BGB) method [22] that matches 3D normals to vessel walls and 2D X-ray gradients back-projected into 3D. The method proposed in Section II is based on *matching of the geometric primitives* and was thus referred as the MGP. Additional registration tests were performed by running consecutively the proposed MGP and BGB methods so as to demonstrate that the combined $MGP + BGB$ can further improve the registration performance. Rigid-body parameters obtained by the MGP method were used as initial parameters for the BGB method.

The compute-intensive MIP-MI method was implemented in CUDA [48] and executed on NVIDIA GeForce GTS 450 graphics card. The vasculature centerline points needed to run the ICP method were obtained by Live-Vessel software [49]. As the extraction of centerline points is controlled by visual feedback, we expect to obtain similar centerline points for vessels in 2D-DSA and 2D-MAX images. Hence, centerline points were extracted only from the 2D-DSA images and then applied to corresponding 2D-MAX images. There were about 14 000 centerline points per 2D image for which the distance transform was precomputed so as to speed up the nearest neighbor search to the projected 3D centerline points [20]. In the BGB method the 3D intensity gradients were extracted using the Canny edge detector, which typically resulted in about 17 000 edge points. The 2D intensity gradients were computed by the central difference kernel.

Parameters of the evaluated state-of-the-art 3D-2D registration methods were experimentally set so as to obtain the best registration performances on the clinical image dataset 1. In the MIP-MI method, the sampling step along the projection rays was 0.375 mm and the intensities were discretized in 64 bins to compute the MI histograms. The ICP had no user-controlled parameters, while in the BGB method the sensitivity of the angle weighting function, similar to (5), was set to $n = 4$.

In all evaluated 3D-2D registration methods, search for the optimal rigid-body parameters $(\mathbf{q}*)$ was performed by Powell's multi-dimensional directional set method [50]. The methods were executed in MATLAB (The MathWorks, Inc., Natick, MA, USA) on an Intel Core i7 CPU 860 @ 2.80 GHz computer with 8 GB memory.

The experiments consisted of registrations of a 3D-DSA image to either a LAT or AP view and simultaneously to both 2D-DSA images. A similar set of experiments was performed by using 2D-MAX instead of 2D-DSA images, i.e., the 3D-DSA image was registered to either a LAT or AP view and simultaneously to both 2D-MAX images. Overall, we performed 24 000 registrations per each of the tested method.

In the following subsections we describe the evaluation of 3D-2D registrations Section IV-A and the parameter settings of the proposed MGP method Section IV-B. The influence of the proposed 3D vessel tree model extraction Section II-A on the performances of the MGP method is analyzed in Section IV-C. Results of quantitative evaluation of the 3D-2D registration methods are reported in Section V.

A. Registration Evaluation

The 3D-2D registration methods were evaluated by standardized evaluation methodologies proposed by van de Kraats *et*

al. [32] and Markelj *et al.* [34], in which mTRE is used as a measure of the accuracy of a 3D-2D registration. The mTRE was computed as the mean distance between 3D vessels' centerline points C_i^{3D} in the "gold standard" position and the position as obtained by a 3D-2D registration method. Following the methodology of van de Kraats *et al.* [32], rigid-body translations and rotations were randomly sampled in the range of $[-20, 20]$ mm and $[-10, 10]$ degrees, respectively, so as to generate initial displacements of the pre-EIGI 3D image from the "gold standard" position in the range of 0-20 mm of mTRE. Twenty initial displacements were generated per each 1 mm subinterval of mTRE, resulting in 400 different displacements for each of the 10 datasets. If mTRE after executing the 3D-2D registration method was below 2 mm, the registration was considered successful. Overall accuracy of the 3D-2D registration was defined as MEAN $\pm$STD of mTRE of all successful registrations. To show the registration accuracy according to Markelj *et al.* [34], the range of initial mTRE displacements was divided into 20 accumulative subintervals 0–1 mm, 0–2 mm,…, 0–20 mm, and for each subinterval the accuracy was calculated as the 95th percentile of mTRE distribution. Capture range (CR) was defined as the first 1 mm subinterval with less than 95% of successful registrations. Success rate (SR) was defined as the overall percentage of successful registrations. CR and SR were used to quantify the robustness of registration methods.

When 3D-DSA images were registered only to a single 2D view (LAT or AP) the mean reprojection distance (mRPD) was computed instead of mTRE. mRPD is defined as the mean of minimum distances between the lines, which pass through the X-ray source and the 3D target points in the registered position, and the corresponding 3D target points in the "gold standard" position [32].

Registration results were presented according to the standardized evaluation protocols [32], [34] as outlined above. The overall registration accuracy, SR, CR and mean execution times were computed over all 10 datasets for each of the evaluated 3D-2D registration method.

B. Parameter Settings

The three parameters of the proposed MGP method were set to following default values $n = 2$, $m = 70$, and $k = 2$. To analyze the influence of these parameters on the performance of the proposed MGP method, one parameter was varied at a time, while the values of other parameters were held fixed at the default values. The parameter settings are given in Table II. The analysis was performed on image dataset 1 for registrations of 3D-DSA to 2D-DSA image(s), either to a single LAT or to both LAT and AP 2D-DSA images simultaneously. Registration accuracy and SR were evaluated for each combination of parameter values.

C. Influence of 3D Vessel Tree Model Extraction

To evaluate the influence of the four-step 3D vessel tree model extraction Section II-A on the performance of the MGP registration method, we varied the global intensity threshold (step 1 in Section II-A. Namely, three different global intensity thresholds were used to obtain three different vessel segmentations, shown as A, B, and C in Fig. 5. B represents the

TABLE II
PARAMETER SETTINGS OF THE PROPOSED MGP METHOD USED IN THE EXPERIMENTS IN SECTION IV-B. THE PARAMETER VALUES SHOWN IN BOLD REPRESENT THE DEFAULT PARAMETER SETTING

Parameter	Parameter settings					
	1	2	3	4	5	6
n	1	**2**	3	4	5	6
m	0	10	30	50	**70**	90
k	0.5	1	1.5	**2**	2.5	3

(a)   (b)

(c)   (d)
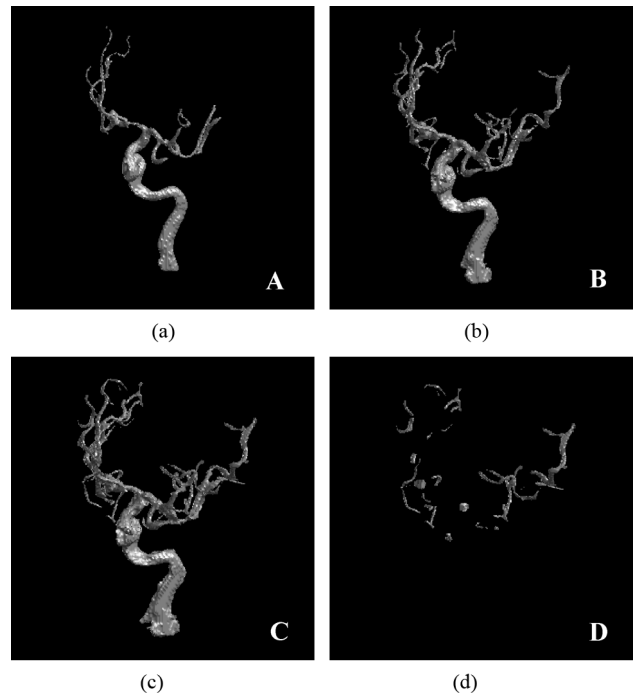
Fig. 5. Volume renderings of four different vessel segmentations of 3D-DSA image in dataset 1. Volume rendering of segmentation A using high global intensity threshold, where mainly large-diameter vessels are visible (a). By lowering the global intensity threshold the small-diameter vessels start to appear (b), (c). Volume rendering of only the small-diameter vessels obtained by removing large-diameter vessels from segmentation C (d).

segmentation by the manually determined threshold. In A the threshold was set higher than in B so that the output segmentation was comprised mainly of large-diameter, high-contrasted vessels. Note that in the 3D-DSA the vessels appear bright. Conversely, in C the threshold was set lower than in B so that the output segmentation included all of the large- and many of the small-diameter vessels. Segmentation D, containing only small-diameter, low-contrasted vessels of the segmentation C, was generated by analyzing the centerline points of segmentations A and C. First, for each centerline point in C the closest point in A was found and the corresponding distance between each pair of centerline points was computed. If the distance was larger than some threshold, then it was assumed that the centerline point in C does not have a corresponding centerline point in A. Finally, parts of segmentation C locally connected to these remaining centerline points were used to generate segmentation D. The vessel segmentation influence was analyzed

TABLE III
MEAN AND STD OF MRPD VALUES OF SUCCESSFUL REGISTRATIONS, SR, CR, AND MEAN EXECUTION TIMES AVERAGED OVER ALL 10 DATASETS FOR FIVE DIFFERENT METHODS REGISTERING A 3D-DSA TO A SINGLE 2D VIEW (LAT OR AP)

View	Method	MEAN ± STD (mm)		SR [%]		CR (mm)		Time (s)
		DSA	MAX	DSA	MAX	DSA	MAX	
LAT	MIP-MI	0.30 ± 0.29	0.64 ± 0.53	77.43	37.18	5	2	84.3
	ICP	0.41 ± 0.34		45.05		0		0.5
	BGB	0.40 ± 0.37	0.41 ± 0.36	52.38	48.43	3	3	11.6
	MGP	0.61 ± 0.37	0.63 ± 0.39	73.23	69.98	5	4	0.5
	MGP+BGB	0.28 ± 0.21	0.31 ± 0.25	79.45	75.23	6	4	15.3
AP	MIP-MI	0.26 ± 0.29	0.68 ± 0.40	92.43	39.73	11	0	52.3
	ICP	0.32 ± 0.25		72.48		1		0.4
	BGB	0.39 ± 0.35	0.47 ± 0.39	58.18	54.75	3	3	10.8
	MGP	0.55 ± 0.29	0.65 ± 0.33	92.23	82.65	11	8	0.5
	MGP+BGB	0.28 ± 0.19	0.37 ± 0.29	95.45	86.8	12	8	11.5

TABLE IV
MEAN AND STD OF MTRE VALUES OF SUCCESSFUL REGISTRATIONS, SUCCESS RATES (SR), CAPTURE RANGES (CR) AND MEAN EXECUTION TIMES AVERAGED OVER ALL 10 CLINICAL DATASETS FOR FIVE DIFFERENT METHODS REGISTERING LAT AND AP VIEWS SIMULTANEOUSLY

Method	MEAN ± STD (mm)		SR [%]		CR (mm)		Time (s)
	DSA	MAX	DSA	MAX	DSA	MAX	
MIP-MI	0.23 ± 0.22	0.41 ± 0.32	96.68	39.63	12	1	118.7
ICP	0.35 ± 0.30		87.33		7		0.7
BGB	0.29 ± 0.29	0.31 ± 0.26	43.98	44.05	2	4	19.5
MGP	0.42 ± 0.23	0.56 ± 0.30	98.63	89.18	19	9	0.7
MGP+BGB	0.20 ± 0.06	0.23 ± 0.10	99.2	90.73	19	12	15.1

on dataset 1 by registering the 3D-DSA to 2D-DSA of a single LAT or both LAT and AP views.

V. RESULTS

A. Registration Results

The performances of 3D-2D registration methods were evaluated with respect to registration accuracy, robustness and execution time Section IV-A. For registrations of a 3D-DSA image to a single 2D view, either the LAT or the AP, the mRPDs are given in Table III, while for registrations of a 3D-DSA image to two 2D views, the mTREs are given in Table IV. The registration accuracy of the MGP method in accumulative subintervals, using either one or two 2D views, is shown in Fig. 6.

1) Registration Accuracy: For both the single and dual view registrations, the registration accuracy of all of the evaluated methods was below 0.75 mm Tables III and IV, i.e., the 3D image voxel size. For 3D-DSA to 2D-DSA registrations, the MIP-MI and $\text{MGP} + \text{BGB}$ methods were the most accurate at about 0.3 and 0.2 mm for single and dual view setups,

respectively. Interestingly, similar registration accuracies were achieved for 3D-DSA to 2D-MAX by using the gradient matching methods (BGB, MGP, $\text{MGP} + \text{BGB}$), while the registration accuracy of MIP-MI was worse at 0.66 and 0.41 mm for single and dual view setups, respectively. The MGP method had a slightly, but insignificantly lower registration accuracy. This was due to the neighborhood-based matching process that reduces the distinctiveness of the SM near the optimal registration (cf. Section V-B).

2) Robustness: As the 2D-DSA segmentation was used for 2D-MAX the results of the ICP method involving 2D-MAX images can be considered as the best case scenario. Surprisingly though, the ICP method achieved the lowest CR among all the evaluated methods in the single view registration scenario. For single LAT view registrations the SR was comparable to the BGB method and was otherwise higher in the single AP view and dual view registrations. Nevertheless, the robustness of ICP and BGB methods was clearly inferior in comparison to other evaluated methods. The proposed MGP method outperformed all of the tested state-of-the-art methods in terms of
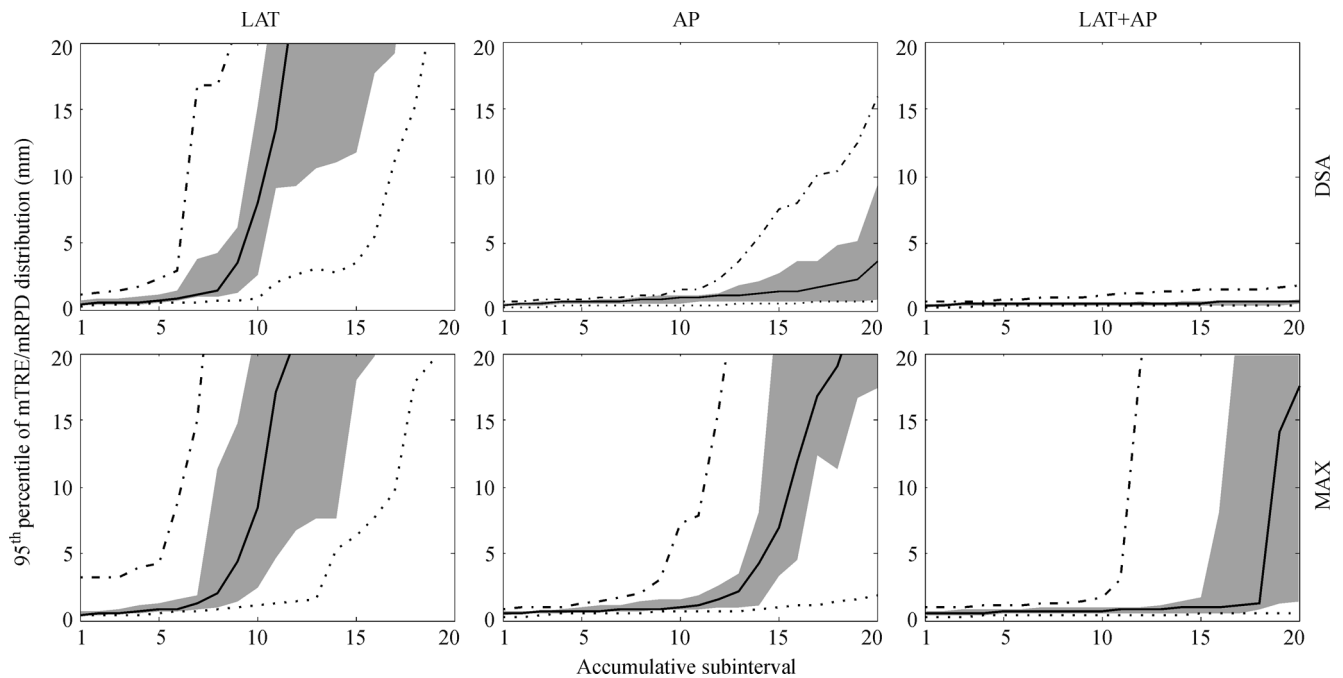
Fig. 6. Registration accuracies of the MGP method defined as 95th percentile of mTRE/mRPD distribution for each of 20 accumulative subintervals of initial mTRE displacements. Minimal, median, and maximal accuracies in each subinterval were calculated across all 10 clinical datasets and is represented by *dashed–dotted, solid,* and *dotted lines*, respectively. *Grey* area denotes the range of registration accuracies between first and third quartile.

SR and CR and proved to be highly robust in all experiments. SR and CR were slightly but consistently improved by using the combined $MGP + BGB$ method. Compared to the MGP and $MGP + BGB$ methods, the MIP-MI method had a similar SR, but lower CR in most of the tests (Tables III and IV), especially for registrations of 3D-DSA to 2D-MAX images. Hence, MIP-MI is not as robust as the proposed MPG method in the case of low vessel-to-background contrast and in the presence of other anatomical structures and interventional tools.

3) Execution Time: Tables III and IV report solely the execution times required by the optimization method to find the rigid-body parameters of the pre-EIGI 3D image. In addition to these times, the ICP method required segmentation of vessels both in 3D and 2D images and computation of the distance transform [20]. In practice, 3D segmentation can be computed prior to EIGI, while 2D segmentation and the distance transform have to be computed during EIGI, which may slow down the procedure. The extraction of a 3D vessel tree model required by the MGP method took up to 5 min but can be performed pre-EIGI. The 2D intensity gradients and corresponding integral images were on average computed in 0.35 s and in 0.8 s for one and two views, respectively. Processing of the 2D image is required only once before the start of the registration process and can be easily optimized to achieve overall execution times of the MGP method below 1 s.

B. Parameter Settings

The proposed novel 3D-2D registration method (referred as MGP) has three parameters n, m, and k, the influence of which on the registration is shown in Fig. 7. Parameter n controls the sensitivity of the angle weighting function (5) and does not have a significant effect on registration accuracy. By increasing
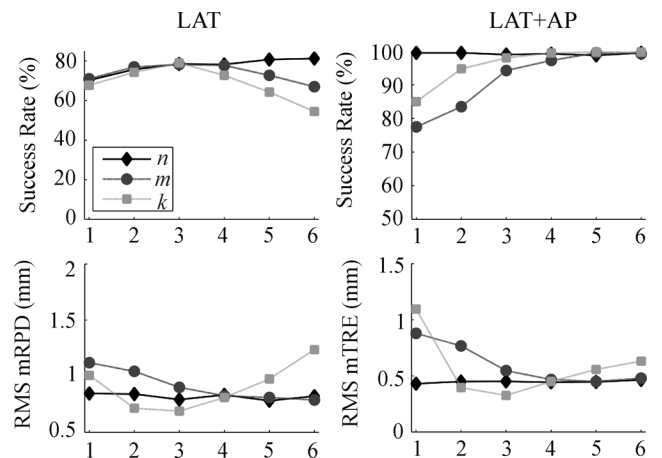
Fig. 7. Registration performances for different settings of parameters n, m, k of the proposed MGP method: success rates *(top)* and the rms of mRPD/mTRE values of successful registrations *(bottom)* for 3D-2D registration of 3D-DSA to a single LAT *(left)* and to LAT+AP *(right)* 2D-DSA images.

n from 1 to 6 a linear increase in SR of up to 5% was observed for registrations of a 3D-DSA to 2D-DSA of a single LAT view, while SR was not affected when both LAT and AP views were used. As expected, reducing the sensitivity to weak matches is important in single view registrations, where depth information is limited. Parameter m defines a set of plausible matches for each of the projected geometric primitives (GPs). For lower $m(< 50)$ a high number of unplausible matches are considered as plausible matches, therefore the MGP method has a higher probability of getting trapped in local maxima. This affects both registration accuracy and SR, which seem to be stable for $m \geq 50$ (settings 4, 5, and 6 in Fig. 7). The constant k controls the size of neighborhood Ω_i for each of the projected GPs.
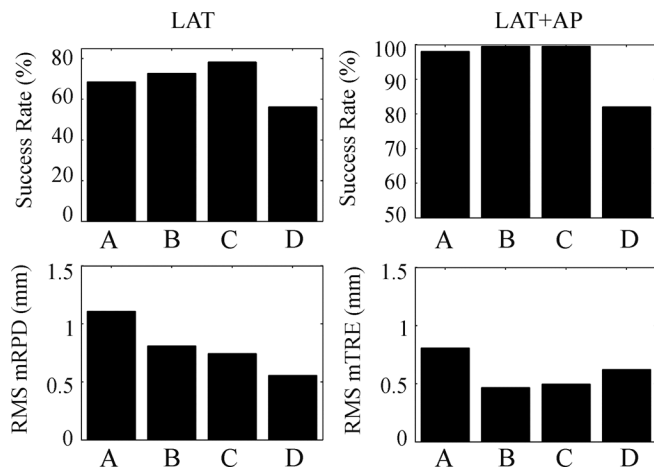
Fig. 8. Registration performances of the proposed MGP method for different 3D vessel tree models in Fig. 5: success rates *(top)* and the rms of mRPD/mTRE values of successful registrations (bottom) of a 3DDSA to a single LAT *(left)* and to LAT+AP views *(right)*.

Higher k and thus larger neighborhoods result in a higher probability that each projected GP will overlap with vessel structures. This is reflected in Fig. 7, where SR increases with k and peaks near $k = 2$. For $k \geq 2$, larger neighborhoods Ω_i may capture more of the surrounding structures that can decrease the resolution of the matching process near the optimal registration and, thus, decrease registration accuracy. Based on discussion above, it is relatively straightforward to identify the optimal parameter values, which were $n = 2$, $m = 70$, and $k = 2$. Moreover, n was set to 2 since it enables a highly efficient implementation of the MGP method by using integral sums Section II-C, while $k = 2$ was chosen as the best trade-off between registration accuracy and SR. In all experiments, parameters values were fixed at the specified optimal values.

C. Influence of 3D Vessel Tree Model Extraction

Extraction of the 3D vessel tree model is an essential part of the proposed MGP method; therefore, its influence on the registration performances is shown in Fig. 8. The 3D model consists of GPs that are extracted from 3D-DSA images in four steps Section II-A, out of which the first contributes most to overall quality of the 3D model. Segmentation of vessels from 3D-DSA images based on global intensity threshold is prone to large errors due to non-uniform spread and/or diffusion of the contrast agent throughout the vessel tree. Fig. 8 shows that SR is generally lower if only small-diameter vessels are segmented Fig. 5(d). The large-diameter vessels Fig. 5(a) seem to contribute most to SR, and by additionally capturing more and more small-diameter vessels (Fig. 5(b) and (c), SR gradually improves. At the same time, registration accuracy improves as more small-diameter vessels are captured by segmentation. The reason is that by also segmenting small-diameter vessels, the 3D vessel tree has a richer structure and, thus, a more precisely defined position of the SM maximum in (4). The possible segmentation artifacts, as a consequence of global-intensity-threshold-based segmentation of noisy images with contrast variations obviously, did not hamper the 3D-2D registrations.

VI. DISCUSSION

This paper has three important contributions: 1) a novel method for 3D-2D rigid registration of cerebral angiograms and 2) a dataset of real clinical images and 3) a quantitative and comparative evaluation of the performances of several 3D-2D rigid registration methods.

A. Novel 3D-2D Registration Method

A method based on matching of geometric primitives (MGP) was proposed in Section II. The 3D-2D registration method first extracts geometric primitives (GPs) from the 3D image, i.e., the vessels' centerline points, orientations and radii, which encode the structure of the 3D vessel tree. The projected GPs are then matched to orientations of 2D intensity gradients using a neighborhood-based similarity measure.

The proposed method was classified as a hybrid 3D-2D registration method. Its development was based on studying the main drawbacks of the state-of-the-art gradient-based methods [22], [34], [51]. These are 1) by considering gradient magnitude directly in the SM, the matching process is driven mainly by magnitude information, 2) gradient magnitude is sensitive to spatial variations of image contrast, and 3) one-to-one gradient matching is very sensitive to small image transformations and thus may not be robust. To overcome these drawbacks, we employed orientation features in a neighborhood-based matching process. Orientation features are relatively independent of image contrast and encode only local image structure [35], [36], [52] while the neighborhood-based matching process increases the probability of detecting corresponding orientation features [21] which then guide the 3D-2D image registration towards the optimal alignment.

B. Clinical Image Database

Translation of novel and existing 3D-2D registration methods into clinical practice can only be achieved after a series of rigorous evaluations, performed on patient images and within a clinical context. The main challenge when using these clinical image databases for quantitative evaluation of 3D-2D registrations is how to obtain the reference or "gold standard" registrations. Typically, manually aligned images are used as the "gold standard" registration. Such "gold standards" are generally less accurate than "gold standards" obtained with fiducial markers. Besides, registration evaluations have to be performed on a larger image database. In the past, 3D-2D registration methods were typically tested on only a few clinical image datasets and with a manually determined "gold standard" [11], [17], [20]. A few image datasets with manual "gold standard" registrations may not be reliable and thus not sufficient for thorough and objective evaluation.

Our clinical image database consisted of 10 datasets of images of patients acquired just before the start of cerebral-EIGI either for aneurysm or AVM treatment. The "gold standard" registrations were obtained by retrospective alignment of fiducial markers integrated into a special headband that each patient wore during the acquisition of images. The resulting error (mTRE) of the "gold standard" registrations for the vessel structures was less than 0.056 mm, which was an order of magnitude lower than the expected error of a 3D-2D registration method.

The obtained "gold standard" thus enables reliable measurements of registration error.

The presented clinical image database with fiducial marker-based "gold standard" registrations is, to the best of our knowledge, so far the most extensive and objective database that serves for quantitative evaluation of 3D-2D registration methods in the context of cerebral EIGI. We believe that 10 image datasets guarantee a faithful evaluation of registration methods and are also representative of the clinical context as they contain two different vascular pathologies of various degrees as well as interventional tools Fig. 3. To motivate further development and evaluation of 3D-2D registration methods for cerebral EIGI the clinical image database is made publicly available and can be found online.[2]

C. Quantitative and Comparative Evaluation of Methods

The clinical image database with known "gold standard" or reference registrations was used to quantitatively evaluate the proposed and three state-of-the-art 3D-2D registration methods Table I. Additional registration tests were performed by running consecutively the MGP and BGB methods $(\text{MGP} + \text{BGB})$.

Registration accuracy of all evaluated methods was below the 3D image voxel size, which was 0.75 mm. The performances of tested methods differed mainly by their sensitivity to poor initialization, sensitivity to image noise and contrast variations, sensitivity to the presence of pathology and presence of interventional tools, etc. The degree of these sensitivities was referred to as robustness, where high robustness meant low sensitivity. Robustness of the evaluated 3D-2D registration methods was expressed by SR and CR Section IV-A, and by comparing the overall performances between the 3D-DSA to 2D-DSA and between the 3D-DSA to 2D-MAX registrations. Compared to 2D-DSA images, the 2D-MAX images manifested a lower vessel-to-background contrast and depicted non-vascular anatomical structures and interventional tools. A 3D-2D registration method was considered robust if it performed equally well on both modalities.

The proposed MGP and the combined $\text{MGP} + \text{BGB}$ methods proved to be the most robust, with more than 69% and 75% of successful registrations in all registration experiments, respectively. The CRs of these two methods were also the highest, ranging up to 12 and 19 mm in respective single and dual view experiments.

Probably the most difficult challenge of a 3D-2D registration method is dealing with nonuniform spread and/or diffusion of contrast agent that causes intensity variations in both 3D and 2D images. The proximal, large-diameter vessels, through which the contrast agent is delivered, typically receive a high amount of contrast agent that reflects in high attenuation of X-rays. This manifests in a high vessel-to-background contrast. Distribution of contrast agent in more distal, small-diameter vessels is mainly governed by the properties of blood flow and/or geometry of the vessel tree. Therefore, the amount of contrast agent delivered to each of these vessels can vary significantly, which results in high contrast variations between distal vessels Fig. 3(b). Vascular pathology can also affect the distribution of contrast agent.

For instance, in dataset 7 Fig. 3(c) the contrast agent accumulated in the large aneurysm, causing most of the small-diameter vessels to appear less prominent. The most difficult case was the registration of 3D-DSA to lateral 2D-MAX image of dataset 5, in which the MAX image had extremely low vessel-to-background contrast. In this case, small-diameter distal vessels were not "captured" by threshold β of the proposed MGP method, but nevertheless, the MGP method performed the best. The performance of the MGP method in such cases can be improved by lowering threshold β. The reason that the proposed MGP method is robust to the above-mentioned image contrast variations, and also to other adverse phenomena, is due to the neighborhood-based matching process relying on corresponding orientation features in 3D and 2D images Section II-B.

The execution time of the proposed MGP method was comparable to the feature-based ICP method and was in the order of a second. The $\text{MGP} + \text{BGB}$ method and BGB methods had mean execution times between 10 and 20 s using a single-threaded implementation. By using a multi-threaded implementation or a dedicated CUDA implementation, the corresponding executions times should be comparable to those of the MGP method. Although, the MIP-MI method was implemented in CUDA, execution times were still at least five times longer than for other methods.

VII. CONCLUSION

In this paper, we presented a novel method for 3D-2D rigid registration of cerebral angiograms. The method is based on matching of geometric primitives, which encode the structure of the 3D vessel tree, to orientations of 2D intensity gradients using a neighborhood-based similarity measure. The main advantage of the proposed method is its robustness to image contrast variations and other adverse phenomena that can hamper the registration process. Besides, the overall execution time in the order of a second makes the method a good candidate for EIGI.

Translation of any 3D-2D registration method into clinical practice requires extensive and rigorous evaluations on real-patient image databases. Therefore, we acquired a clinical image database representative of cerebral-EIGI and established a highly accurate "gold standard" registration that enables objective quantitative evaluation of 3D-2D rigid registration methods. The quantitative and comparative evaluation of three state-of-the-art methods showed that the performance of the proposed method best met the demands of cerebral EIGI. The image database and registration results of the evaluated methods are publicly available and can be found online.[2]

REFERENCES

[1] H. Schmitt, M. Grass, R. Suurmond, T. Köhler, V. Rasche, S. Hähnel, and S. Heiland, "Reconstruction of blood propagation in three-dimensional rotational X-ray angiography (3D-RA)," *Comput. Med. Imaging. Graph.*, vol. 29, no. 7, pp. 507–520, Oct. 2005.

[2] A. D. Copeland, R. S. Mangoubi, M. N. Desai, S. K. Mitter, and A. M. Malek, "Spatio-temporal data fusion for $3D + T$ image reconstruction in cerebral angiography," *IEEE Trans. Med. Imag.*, vol. 29, no. 6, pp. 1238–1251, Jun. 2010.

[3] P. Markelj, D. Tomazevic, B. Likar, and F. Pernuš, "A review of 3D/2D registration methods for image-guided interventions," *Med. Image. Anal.*, vol. 16, no. 3, pp. 642–661, Apr. 2012.

[4] M. Söderman, D. Babic, R. Homan, and T. Andersson, "3D roadmap in neuroangiography: Technique and clinical interest," *Neuroradiology*, vol. 47, no. 10, pp. 735–740, Oct. 2005.

[5] D. Ruijters, R. Homan, P. Mielekamp, P. van de Haar, and D. Babic, "Validation of 3D multimodality roadmapping in interventional neuroradiology," *Phys. Med. Biol.*, vol. 56, no. 16, pp. 5335–5354, Aug. 2011.

[6] M. V. N. Truong, A. Aslam, M. Ginks, C. A. Rinaldi, R. Rezavi, G. P. Penney, and K. S. Rhode, "2D-3D registration of cardiac images using catheter constraints," *Comput. Cardiol.*, pp. 605–608, 2009.

[7] J. V. Byrne, C. Colominas, J. Hipwell, T. Cox, J. A. Noble, G. P. Penney, and D. J. Hawkes, "Assessment of a technique for 2D-3D registration of cerebral intra-arterial angiography," *Br. J. Radiol.*, vol. 77, no. 914, pp. 123–128, Feb. 2004.

[8] S. Demirci, M. Baust, O. Kutter, F. Manstad-Hulaas, H.-H. Eckstein, and N. Navab, "Disocclusion-based 2D-3D registration for aortic interventions," *Comput. Biol. Med.*, vol. 43, no. 4, pp. 312–322, May 2013.

[9] J. H. Hipwell, G. P. Penney, R. A. McLaughlin, K. Rhode, P. Summers, T. C. Cox, J. V. Byrne, J. A. Noble, and D. J. Hawkes, "Intensity-based 2-D-3-D registration of cerebral angiograms," *IEEE Trans. Med. Imag.*, vol. 22, no. 11, pp. 1417–1426, Nov. 2003.

[10] E. Kerrien, M.-O. Berger, E. Maurincomme, L. Launay, R. Vaillant, and L. Picard, "Fully automatic 3D/2D subtracted angiography registration," in *Medical Image Computing and Comput.-Assisted Intervention—MICCAI 1999*. London: U.K., 1999, pp. 664–671.

[11] R. A. McLaughlin, J. Hipwell, D. J. Hawkes, J. A. Noble, J. V. Byrne, and T. C. Cox, "A comparison of a similarity-based and a feature-based 2-D-3-D registration method for neurointerventional use," *IEEE Trans. Med. Imag.*, vol. 24, no. 8, pp. 1058–1066, Aug. 2005.

[12] M. J. van der Bom, S. Klein, M. Staring, R. Homan, L. W. Bartels, and J. P. W. Pluim, "Evaluation of optimization methods for intensity-based 2D-3D registration in x-ray guided interventions," in *Proc. SPIE*, Orlando, FL, 2011, vol. 7962, pp. 796223–796223-15.

[13] A. C. S. Chung, W. M. Wells, III, A. Norbash, and W. E. L. Grimson, "Multi-modal image registration by minimizing Kullback-Leibler distance," in *Medical Image Computing and Computer-Assisted Intervention—MICCAI 2002*. Berlin, Germany: Springer, 2002, pp. 525–532.

[14] Y. Kita, D. L. Wilson, and A. Noble, "Real-time registration of 3D cerebral vessels to X-ray angiograms," in *Medical Image Computing and Comput.-Assisted Intervention—MICCAI 1998*. Berlin, Germany: Springer, vol. 1496, pp. 1125–1133.

[15] E. Bullitt, A. Liu, S. R. Aylward, C. Coffey, J. Stone, S. K. Mukherji, K. E. Muller, and S. M. Pizer, "Registration of 3D cerebral vessels with 2D digital angiograms: Clinical evaluation," *Acad. Radiol.*, vol. 6, no. 9, pp. 539–546, Sep. 1999.

[16] J. Feldmar, N. Ayache, and F. Betting, "3D-2D projective registration of free-form curves and surfaces," *Comput. Vis. Image. Understand.*, vol. 65, no. 3, pp. 403–424, Mar. 1997.

[17] M. Groher, T. F. Jakobs, N. Padoy, and N. Navab, "Planning and intraoperative visualization of liver catheterizations: New CTA protocol and 2D-3D registration method," *Acad. Radiol.*, vol. 14, no. 11, pp. 1325–1340, 2007.

[18] M. Groher, F. Bender, R.-T. Hoffmann, and N. Navab, "Segmentation-driven 2D-3D registration for abdominal catheter interventions," in *Medical Image Computing and Comput.-Assisted Intervention—MICCAI 2007*. Berlin, Germany: Medical Image Computing and Comput.-Assisted Intervention—MICCAI 2007 , 2007, vol. 10, pp. 527–535.

[19] M. Groher, D. Zikic, and N. Navab, "Deformable 2D-3D registration of vascular structures in a one view scenario," *IEEE Trans. Med. Imag.*, vol. 28, no. 6, pp. 847–860, Jun. 2009.

[20] D. Rivest-Hénault, H. Sundar, and M. Cheriet, "Nonrigid 2D/3D registration of coronary artery models with live fluoroscopy for guidance of cardiac interventions," *IEEE Trans. Med. Imag.*, vol. 31, no. 8, pp. 1557–1572, Aug. 2012.

[21] U. Mitrovic, P. Markelj, B. Likar, Z. Milošević, and F. Pernuš, "Gradient-based 3D-2D registration of cerebral angiograms," *Proc. SPIE*, pp. 79621P–79621P-8.

[22] D. Tomazevic, B. Likar, T. Slivnik, and F. Pernuš, "3-D/2-D registration of CT and MR to X-ray images," *IEEE Trans. Med. Imag.*, vol. 22, no. 11, pp. 1407–1416, Nov. 2003.

[23] P. Markelj, D. Tomazevic, F. Pernuš, and B. Likaaaar, "Robust gradient-based 3-D/2-D registration of CT and MR to X-ray images," *IEEE Trans. Med. Imag.*, vol. 27, no. 12, pp. 1704–1714, Dec. 2008.

[24] H. M. Chan, A. C. S. Chung, S. C. H. Yu, and W. M. Wells, III, "2D-3D vascular registration between digital subtraction angiographic (DSA) and magnetic resonance angiographic (MRA) images," in *Proc. IEEE Int. Symp. Biomed. Imag.: Nano to Macro*, 2004, vol. 1, pp. 708–711.

[25] D. Ruijters, B. M. ter Haar Romeny, and P. Suetens, "Vesselness-based 2D-3D registration of the coronary arteries," *Int. J. Comput. Assist. Radiol. Surg.*, vol. 4, no. 4, pp. 391–397, Jun. 2009.

[26] G.-A. Turgeon, G. Lehmann, G. Guiraudon, M. Drangova, D. Holdsworth, and T. Peters, "2D-3D registration of coronary angiograms for cardiac procedure planning and guidance," *Med. Phys.*, vol. 32, no. 12, pp. 3737–3749, Dec. 2005.

[27] J. Jomier, E. Bullitt, M. Van Horn, C. Pathak, and S. R. Aylward, "3D/2D model-to-Image registration applied to tips surgery," in *Medical Image Computing and Computer-Assisted Intervention—MICCAI 2006*. Berlin, Germany: Springer, 2006, vol. 9, pp. 662–669.

[28] M. Groher, M. Baust, D. Zikic, and N. Navab, "Monocular deformable model-to-image registration of vascular structures," in *WBIR'10 Proceedings of the 4th International Conference on Biomedical Image Registration* . Berlin, Germany: Springer, 2010, pp. 37–47.

[29] U. Mitrovic, Z. Špiclin, B. Likar, and F. Pernuš, "Method for 3D-2D registration of vascular images: Application to 3D contrast agent flow visualization," in *Clinical Image-Based Procedures. From Planning to Intervention*, K. Drechsler, M. Erdt, M. G. Linguraru, C. O. Laura, K. Sharma, R. Shekhar, and S. Wesarg, Eds. Berlin, Germany: Springer, 2013, pp. 50–58.

[30] M. Vermandel, N. Betrouni, J.-Y. Gauvrit, D. Pasquier, C. Vasseur, and J. Rousseau, "Intrinsic 2D/3D registration based on a hybrid approach: Use in the radiosurgical imaging process," *Cell. Mol. Biol.*, vol. 52, no. 6, pp. 44–53, 2006.

[31] D. Tomazevic, B. likar, and F. Pernuš, "Gold standard' data for evaluation and comparison of 3D/2D registration methods," *Comput. Aid. Surg.*, vol. 9, no. 4, pp. 137–144, 2004.

[32] E. an dde Kraats, G. Penney, D. Tomazevic, T. van Walsum, and W. Niessen, "Standardized evaluation methodology for 2-D-3-D registration ," *IEEE Trans. Med. Imag.*, vol. 24, no. 9, pp. 1177–1189, Sep. 2005.

[33] S. A. Pawiro, P. Markelj, F. Pernuš, C. Gendrin, M. Figl, C. Weber, F. Kainberger, I. Noebauer-Huhmann, H. Bergmeister, M. Stock, D. Georg, H. Bergmann, and W. Birkfellner, "Validation for 2D/3D registration I: A new gold standard data set," *Med. Phys.*, vol. 38, no. 3, pp. 1481–1490, Mar. 2011.

[34] P. Markelj, B. Likar, and F. Pernuš, "Standardized evaluation methodology for 3D/2D registration based on the visible human data set," *Med. Phys.*, vol. 37, no. 9, pp. 4643–4647, Sep. 2010.

[35] C. F. Olson and D. P. Huttenlocher, "Automatic target recognition by matching oriented edge pixels," *IEEE Trans. Image Process.*, vol. 6, no. 1, pp. 103–113, Jan. 1997.

[36] S. Hinterstoisser, C. Cagniart, S. Ilic, P. Sturm, N. Navab, P. Fua, and V. Lepetit, "Gradient response maps for real-time detection of texture-less objects," *IEEE Trans. Pattern Anal. Mach. Intell.*, vol. 34, no. 5, pp. 876–888, May 2012.

[37] T. Lee, R. Kashyap, and C. Chu, "Building skeleton models via 3-D medial surface/axis thinning algorithms," *CVGIP-Graph. Model. Imag.*, vol. 56, no. 6, pp. 462–478, Nov. 1994.

[38] K. Krissian, G. Malandain, N. Ayache, R. Vaillant, and Y. Trousset, "Model-based detection of tubular structures in 3D images," *Comput. Vis. Image. Understand.*, vol. 80, no. 2, pp. 130–171, Nov. 2000.

[39] S. R. Aylward and E. Bullitt, "Initialization, noise, singularities, and scale in height ridge traversal for tubular object centerline extraction," *IEEE Trans. Med. Imag.*, vol. 21, no. 2, pp. 61–75, Feb. 2002.

[40] S. Cetin, A. Demir, A. Yezzi, M. Degertekin, and G. Unal, "Vessel tractography using an intensity based tensor model with branch detection," *IEEE Trans. Med. Imag.*, vol. 32, no. 2, pp. 348–363, Feb. 2013.

[41] J. P. Lewis, "Fast normalized cross-correlation," in *Proc. Vis. Interface*, 1995, pp. 120–123.

[42] J. Fitzpatrick, J. West, and C. Maurer, "Predicting error in rigid-body point-based registration," *IEEE Trans. Med. Imag.*, vol. 17, no. 5, pp. 694–702, Oct. 1998.

[43] C. B. Bose and I. Amir, "Design of fiducials for accurate registration using machine vision," *IEEE Trans. Pattern Anal. Mach. Intell.*, vol. 12, no. 12, pp. 1196–1200, Dec. 1990.

[44] G. Chiorboli and G. P. Vecchi, "Comments on 'Design of fiducials for accurate registration using machine vision'," *IEEE Trans. Pattern Anal. Mach. Intell.*, vol. 15, no. 12, pp. 1330–1332, Dec. 1993.

[45] G. Shechter, B. Shechter, J. R. Resar, and R. Beyar, "Prospective motion correction of X-ray images for coronary interventions," *IEEE Trans. Med. Imag.*, vol. 24, no. 4, pp. 441–450, Apr. 2005.

[46] A. M. Dumay, J. C. Reiber, and J. J. Gerbrands, "Determination of optimal angiographic viewing angles: Basic principles and evaluation study," *IEEE Trans. Med. Imag.*, vol. 13, no. 1, pp. 13–24, Jan. 1994.

[47] J. P. W. Pluim, J. B. A. Maintz, and M. A. Viergever, "Mutual-information-based registration of medical images: A survey," *IEEE Trans. Med. Imag.*, vol. 22, no. 8, pp. 986–1004, Aug. 2003.

[48] C. Gendrin, H. Furtado, C. Weber, C. Bloch, M. Figl, S. A. Pawiro, H. Bergmann, M. Stock, G. Fichtinger, D. Georg, and W. Birkfellner, "Monitoring tumor motion by real time 2D/3D registration during radiotherapy," *Radiother. Oncol.*, vol. 102, no. 2, pp. 274–280, Feb. 2012.

[49] K. Poon, G. Hamarneh, and R. Abugharbieh, "Live-vessel: Extending livewire for simultaneous extraction of optimal medial and boundary paths in vascular images," *Med. Image. Comput. Comput. Assist. Interv.*, vol. 10, pp. 444–451, 2007.

[50] M. J. D. Powell, "An efficient method for finding the minimum of a function of several variables without calculating derivatives," *Comput. J.*, vol. 7, no. 2, pp. 155–162, Jan. 1964.

[51] H. Livyatan, Z. Yaniv, and L. Joskowicz, "Gradient-based 2-D/3-D rigid registration of fluoroscopic X-ray to CT," *IEEE Trans. Med. Imag.*, vol. 22, no. 11, pp. 1395–1406, Nov. 2003.

[52] D. G. Lowe, "Distinctive image features from scale-invariant keypoints," *Int. J. Comput. Vis.*, vol. 60, no. 2, pp. 91–110, Nov. 2004.